Electronic Supplementary Information (ESI)

Logic gate behavior and intracellular application of a fluorescent molecular switch for the detection of Fe^{3+} and cascade sensing of F^- in pure aqueous media

Romi Dwivedi[a], Divya P. Singh[a], Saumya Singh[a], Ashish K. Singh[b], Brijesh S. Chauhan[c], S. Srikrishna[c], Vinod P. Singh[a]*.

[a] Department of Chemistry, Institute of Science, Banaras Hindu University, Varanasi-221005 (India)

[b]School of Materials Science and Technology, Indian Institute of Technology (Banaras Hindu University), Varanasi-221005, (India)

[c] Department of Bio Chemistry, Institute of Science, Banaras Hindu University, Varanasi-221005 (India)

**E mail: singvp@yahoo.co.in*

Table of Contents

Fig. S1 ^{1}H NMR spectra of APHN.

Fig. S2 ^{13}C NMR spectra of APHN.

Fig. S3 ^{1}H NMR spectra of RAPHN

Fig. S4 ^{13}C NMR spectra of RAPHN.

Fig. S5 HR-MS spectra of APHN showing molecular ion peak $[M+H]^+$ at 418.15..

Fig. S6 HR-MS spectra of RAPHN showing molecular ion peak $[M+H]^+$ at 422.18.

Fig. S7 HR-MS spectra of RAPHN-Fe^{3+} showing molecular ion peak $[M+Na]^+$ at 765.94.

Fig. S8 Fluorescence emission spectra of RAPHN upon the addition of various salts of Fe^{3+} ions at λ_{ex}: 285 nm.

Fig. S9 Effect of pH (2-12) on the fluorescence spectra of RAPHN (0.5 μM) + Fe^{3+} (5 μM) at λ_{ex}: 285 nm.

Fig. S10 Picture showing the interaction of F^- ion with RAPHN in the presence and absense of Fe^{3+} ions under UV light (1=RAPHN, 2=RAPHN+Fe^{3+}, 3=RAPHN+Fe^{3+}+F^-, 4=RAPHN+F^-).

Fig. S11 Fluorescence spectra showing interaction of F^- with RAPHN in the presence and absense of Fe^{3+} ions.

Fig. S12 Emission intensities of RAPHN (0.5 μM) as a function of [Fe^{3+}] at λ_{em}: 369 nm. The detection limit is 2.49×10^{-7} M. ($R^2 = 0.99097$).

Fig. S13 Emission intensities of RAPHN-Fe^{3+} as a function of [F^-] at λ_{em}: 369 nm. The detection limit is 1.09×10^{-7} M. ($R^2 = 0.99157$).

Fig. S14 Benesi–Hildebrand expression fitting of fluorescence titration curve considering 2:1 (M: L) complexation for RAPHN-Fe^{3+} at λ_{em}: 369 nm ($R^2 = 0.99041$).

Reagents
Instruments
Computational details
References

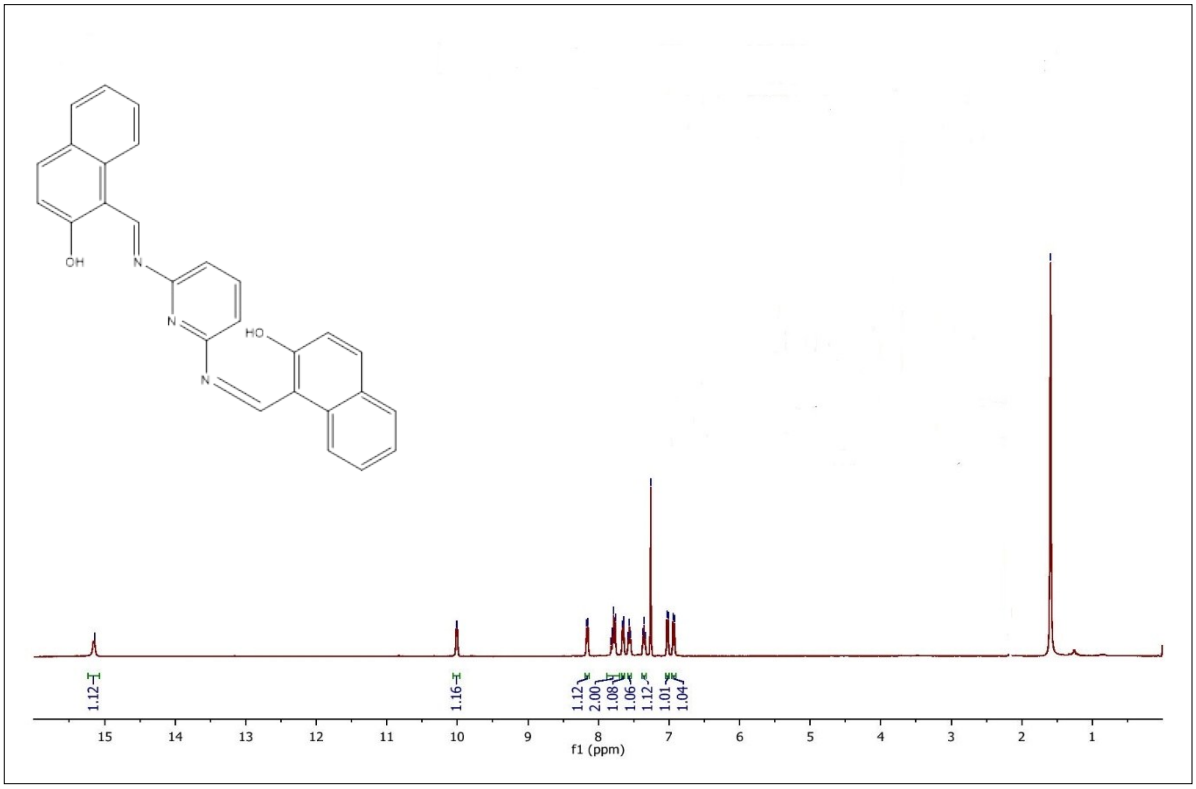

Fig. S1 ^{1}H NMR spectra of APHN.

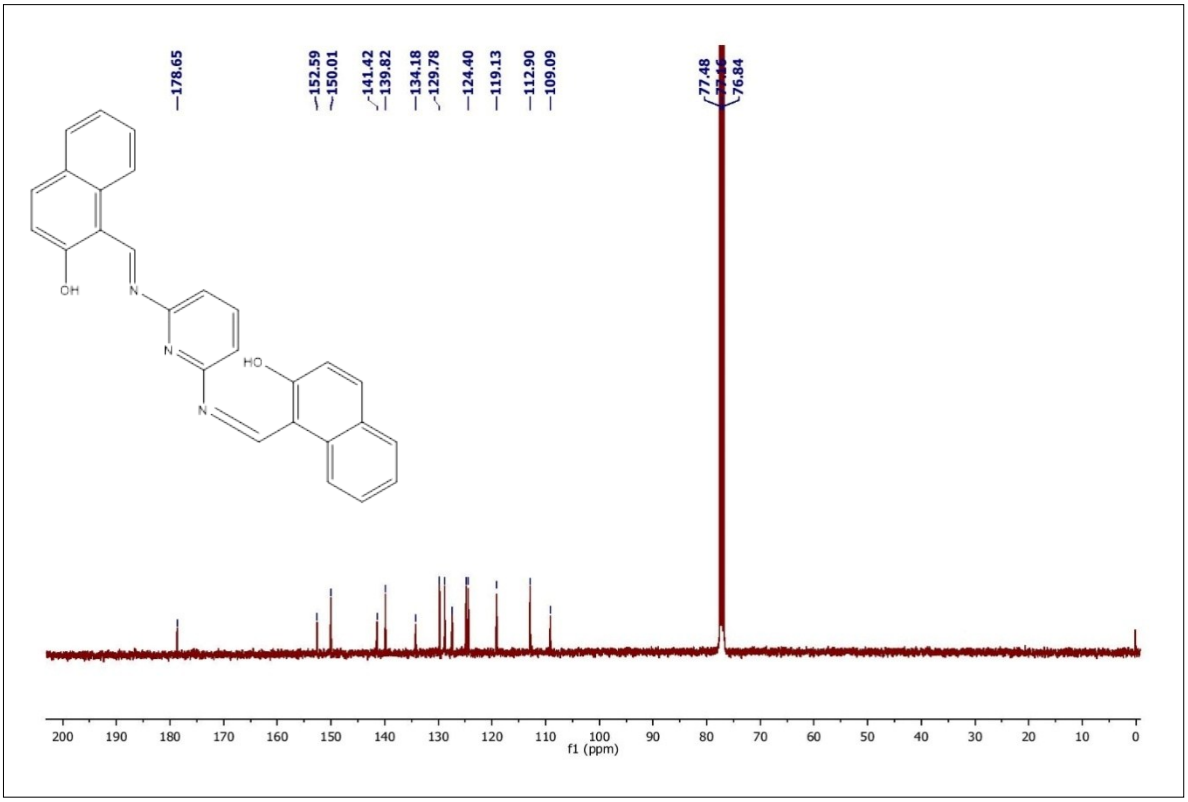

Fig. S2 ^{13}C NMR spectra of APHN.

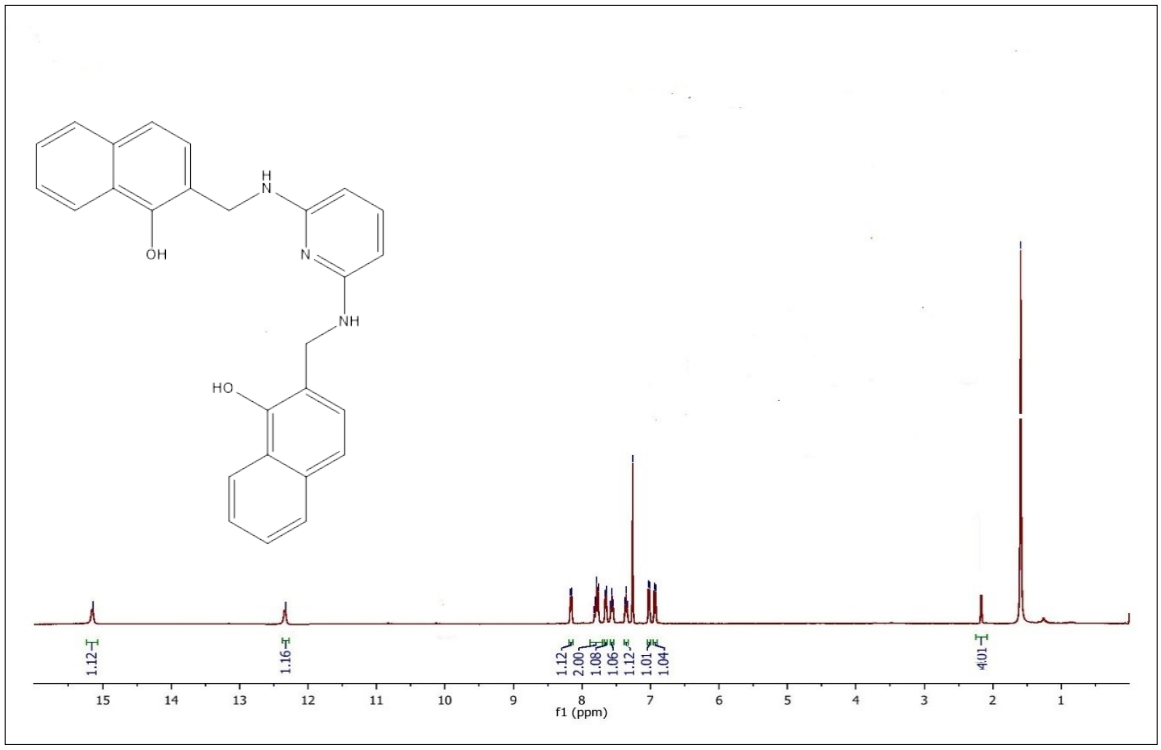

Fig. S3 ^{1}H NMR spectra of RAPHN.

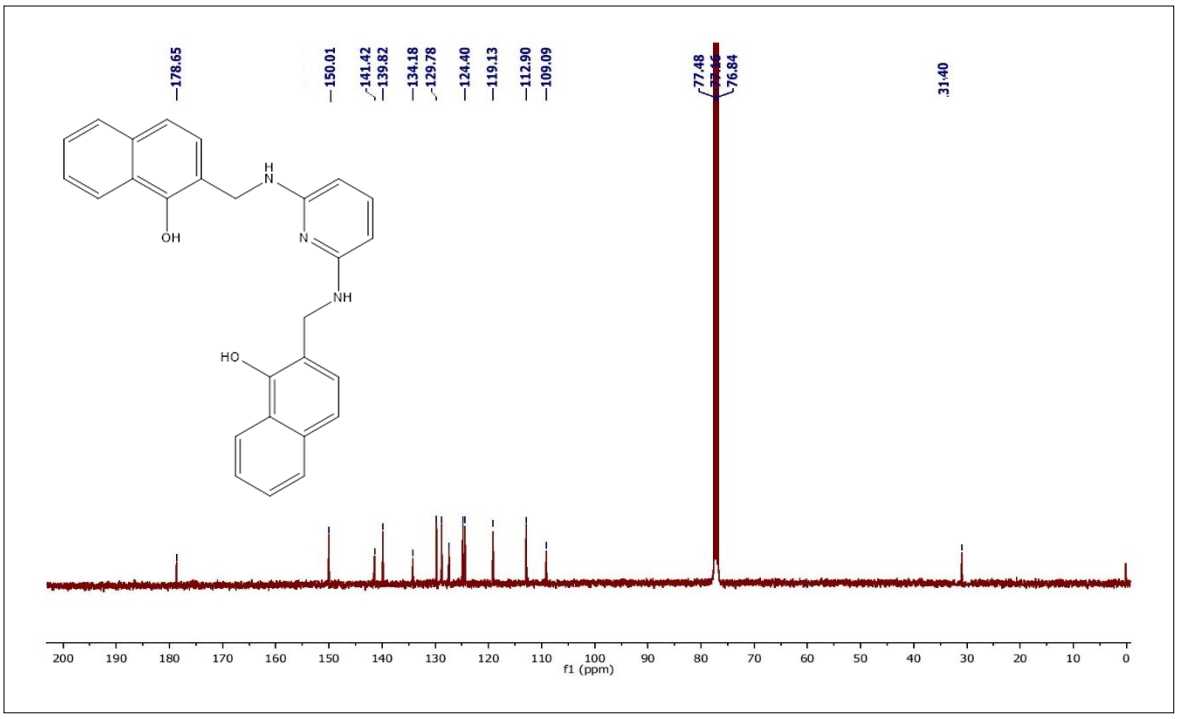

Fig. S4 ^{13}C NMR spectra of RAPHN.

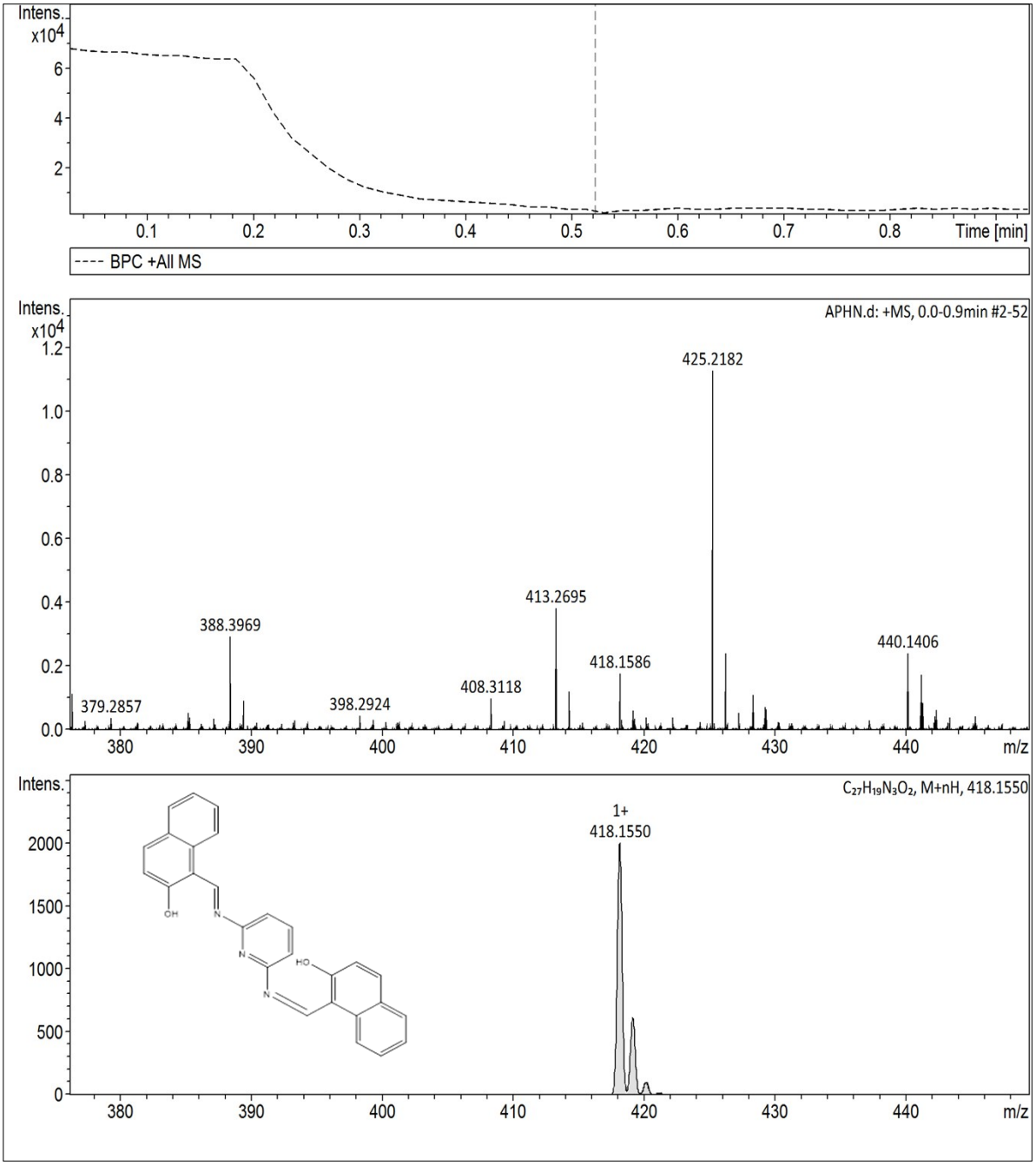

Fig. S5 HR-MS spectra of APHN showing molecular ion peak $[M+H]^+$ at 418.15.

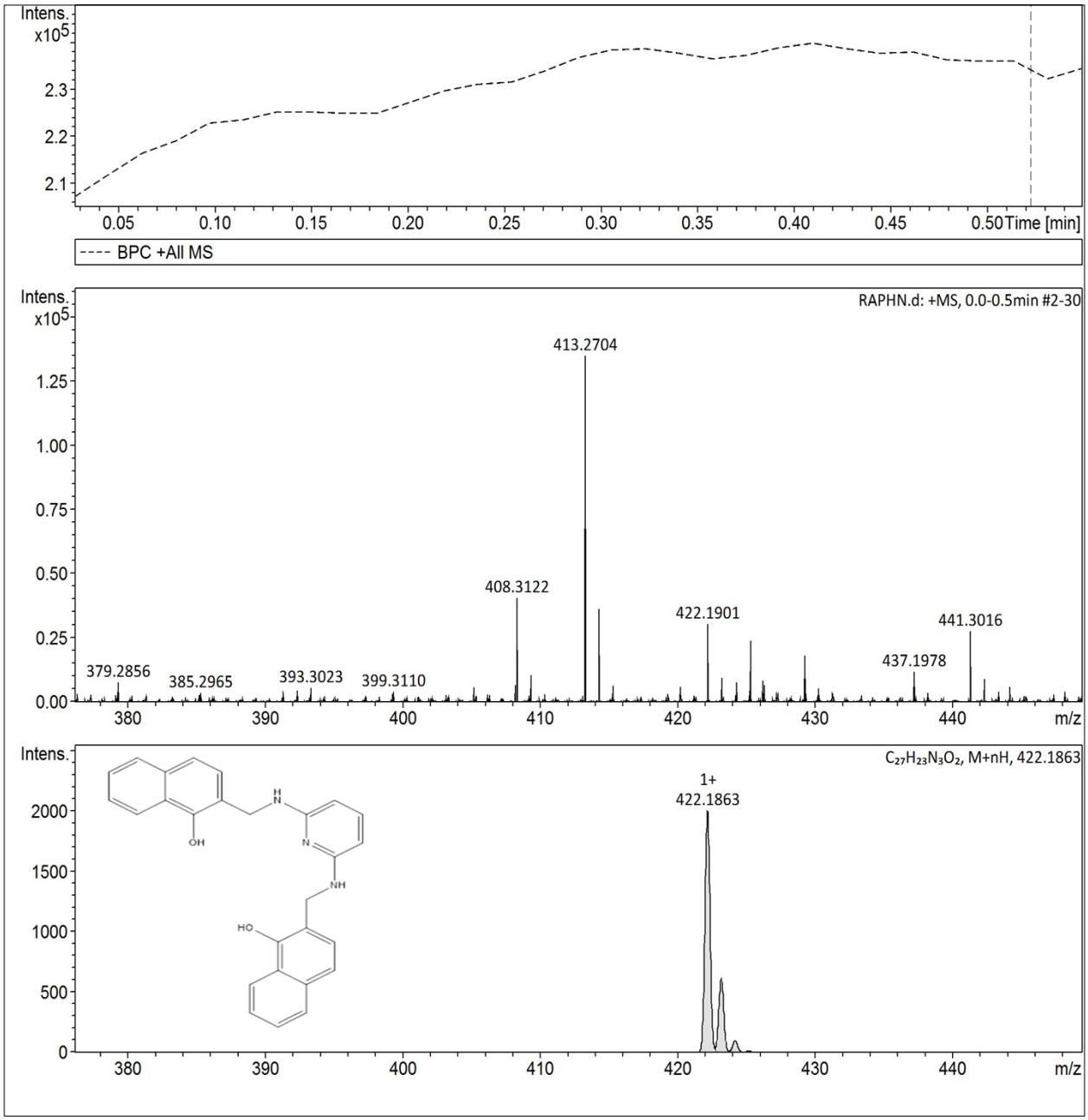

Fig. S6 HR-MS spectra of RAPHN showing molecular ion peak $[M+H]^+$ at 422.18.

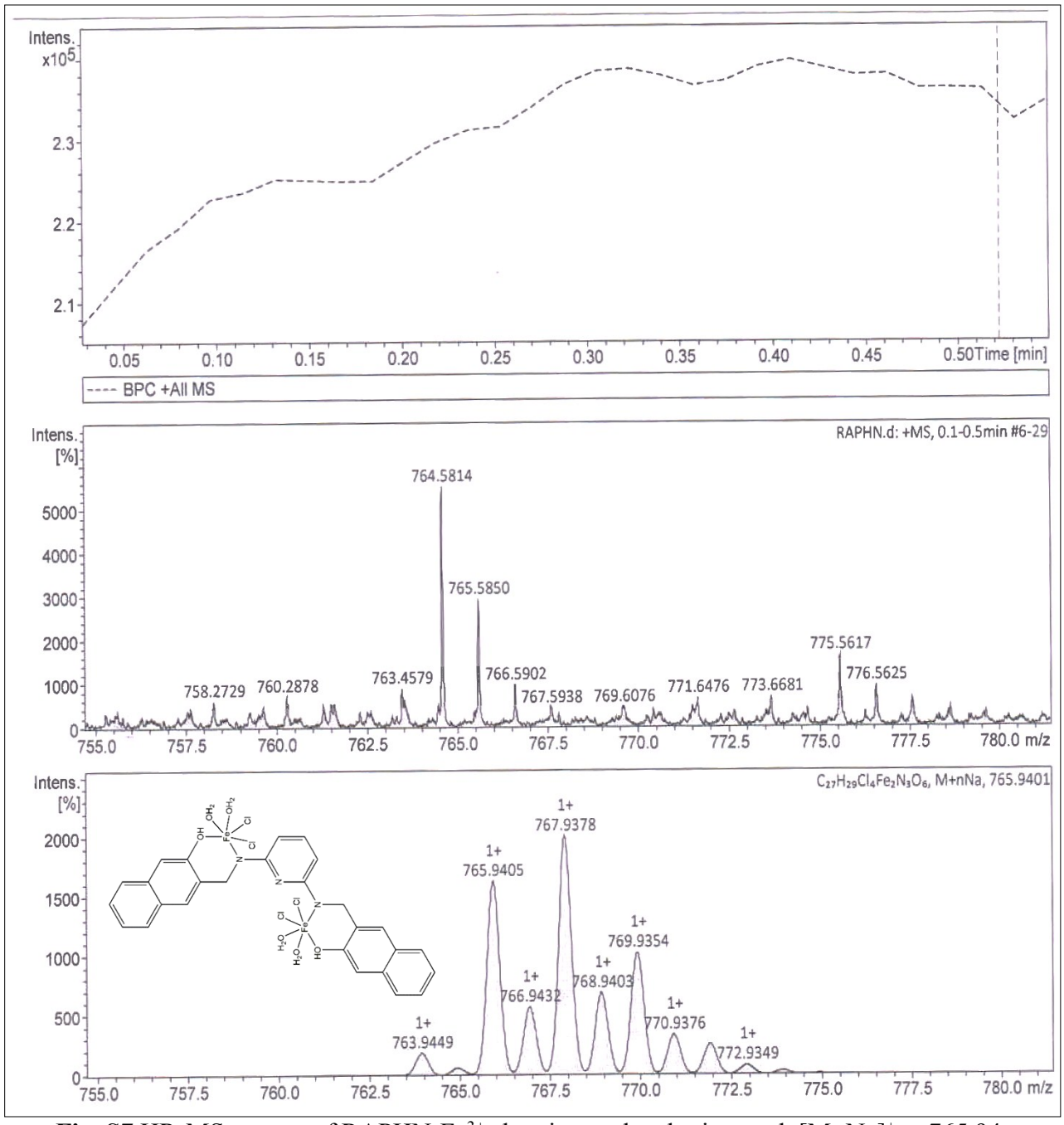

Fig. S7 HR-MS spectra of RAPHN-Fe^{3+} showing molecular ion peak $[M+Na]^+$ at 765.94.

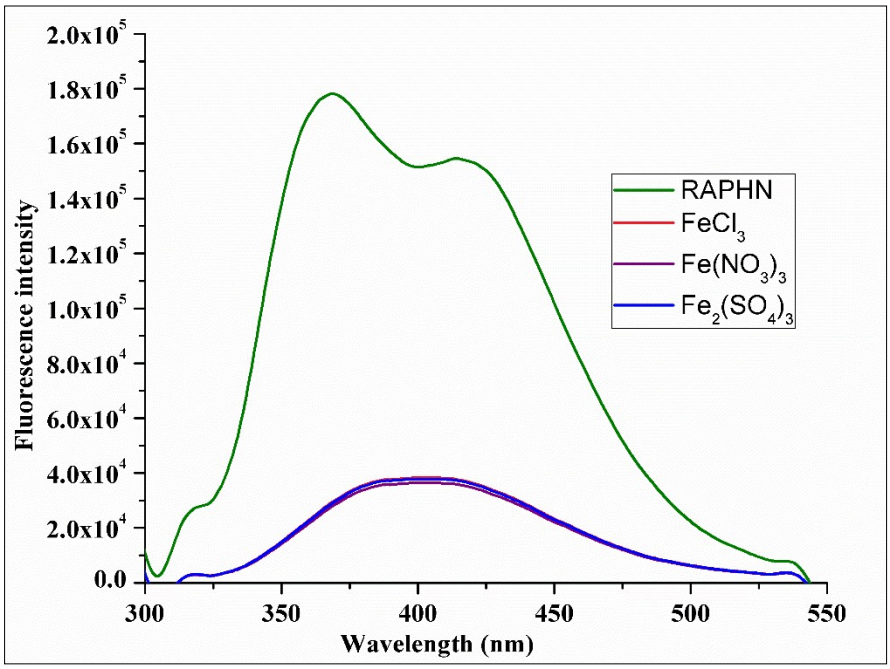

Fig. S8 Fluorescence emission spectra of RAPHN upon the addition of various salts of Fe^{3+} ions at λ_{ex}: 285 nm.

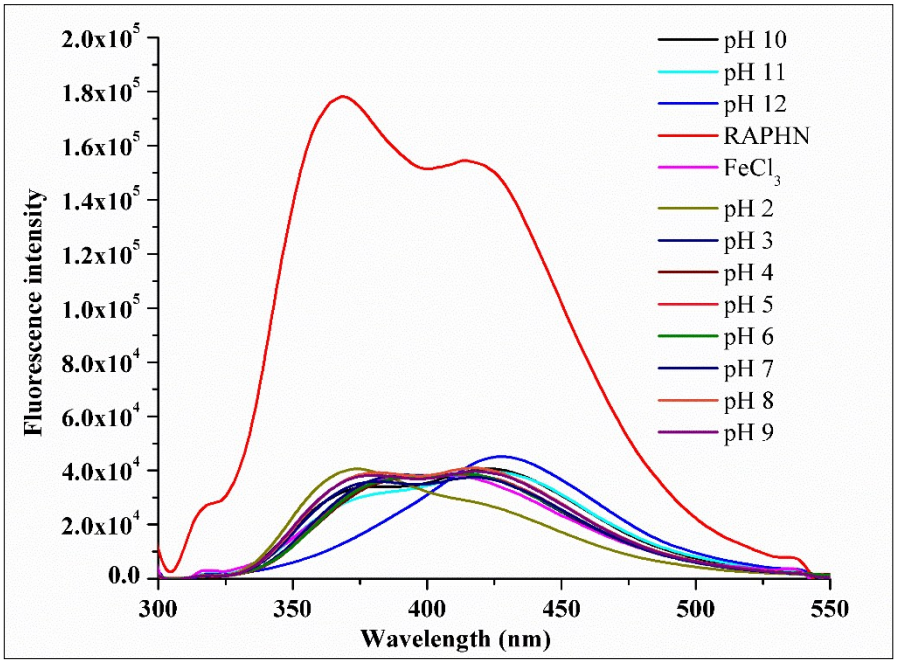

Fig. S9 Effect of pH (2-12) on the fluorescence spectra of RAPHN (0.5 µM) + Fe^{3+} (5 µM) at λ_{ex}: 285 nm.

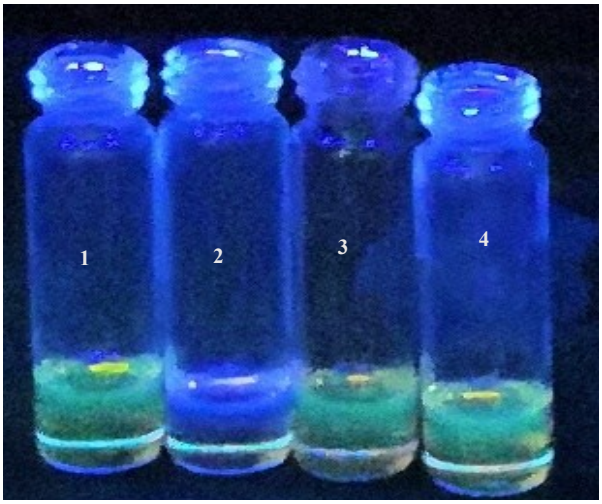

Fig. S10 Picture showing the interaction of F^- ion with RAPHN in the presence and absense of Fe^{3+} ions under UV light (1=RAPHN, 2=RAPHN+Fe^{3+}, 3=RAPHN+Fe^{3+}+F^-, 4=RAPHN+F^-).

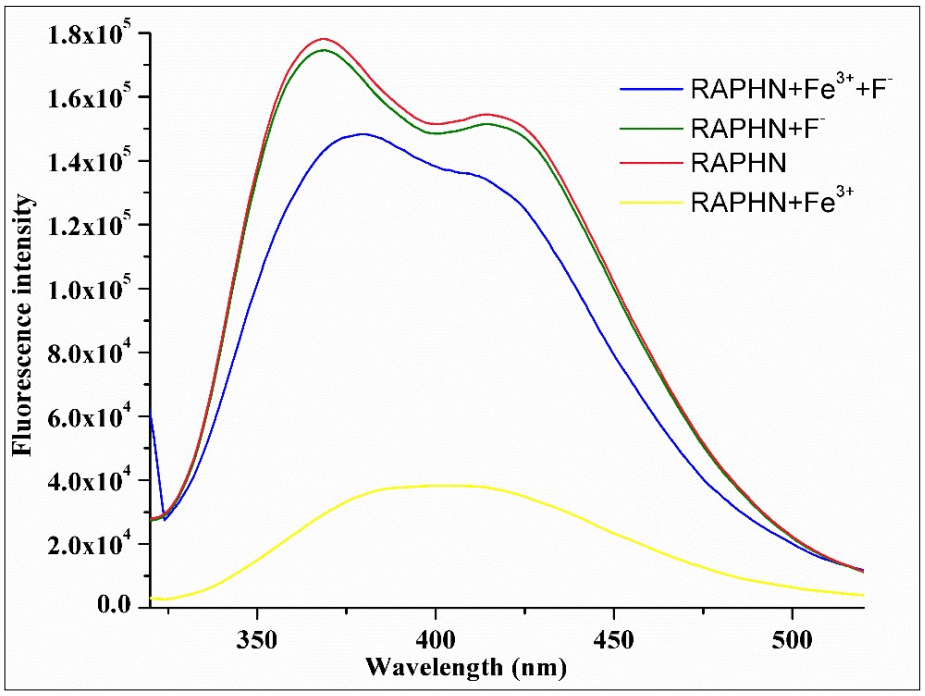

Fig. S11 Fluorescence spectra showing interaction of F^- with RAPHN in the presence and absense of Fe^{3+} ions.

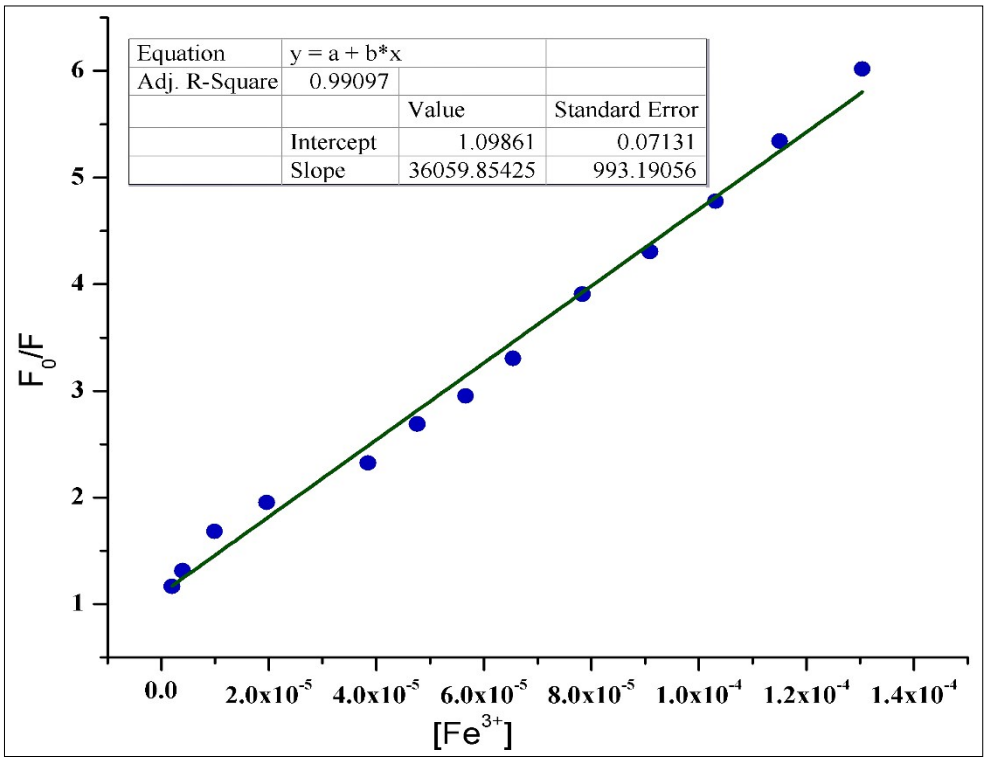

Fig. S12 Emission intensities of RAPHN (0.5 μM) as a function of $[Fe^{3+}]$ at λ_{em}: 369 nm. The detection limit is 2.49×10^{-7} M. ($R^2 = 0.99097$).

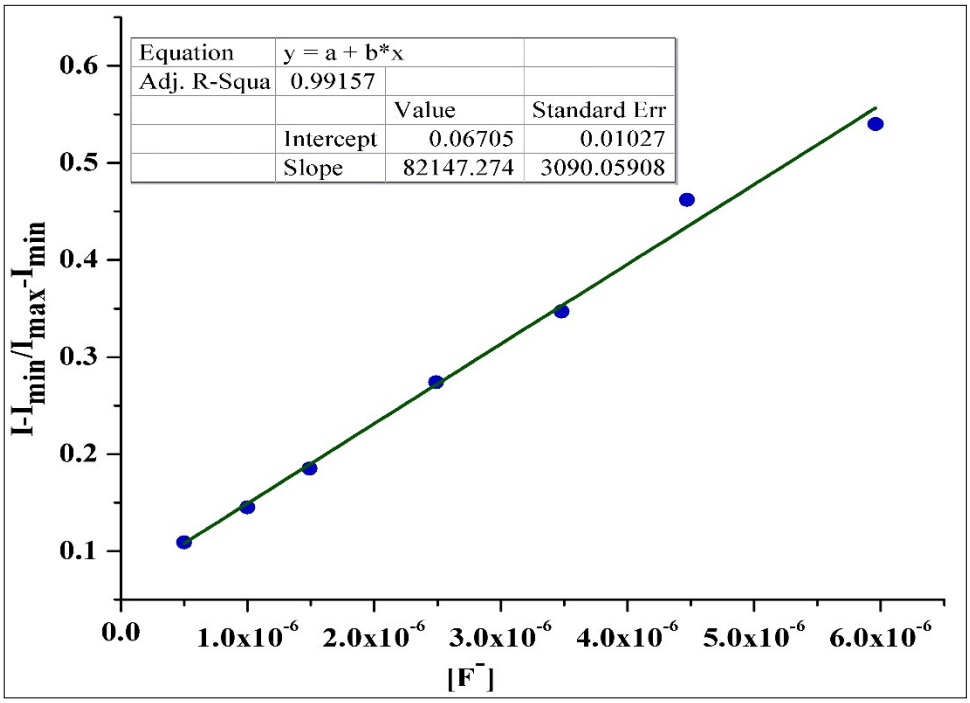

Fig. S13 Emission intensities of RAPHN-Fe^{3+} as a function of $[F^-]$ at λ_{em}: 369 nm. The detection limit is 1.09×10^{-7} M. ($R^2 = 0.99157$).

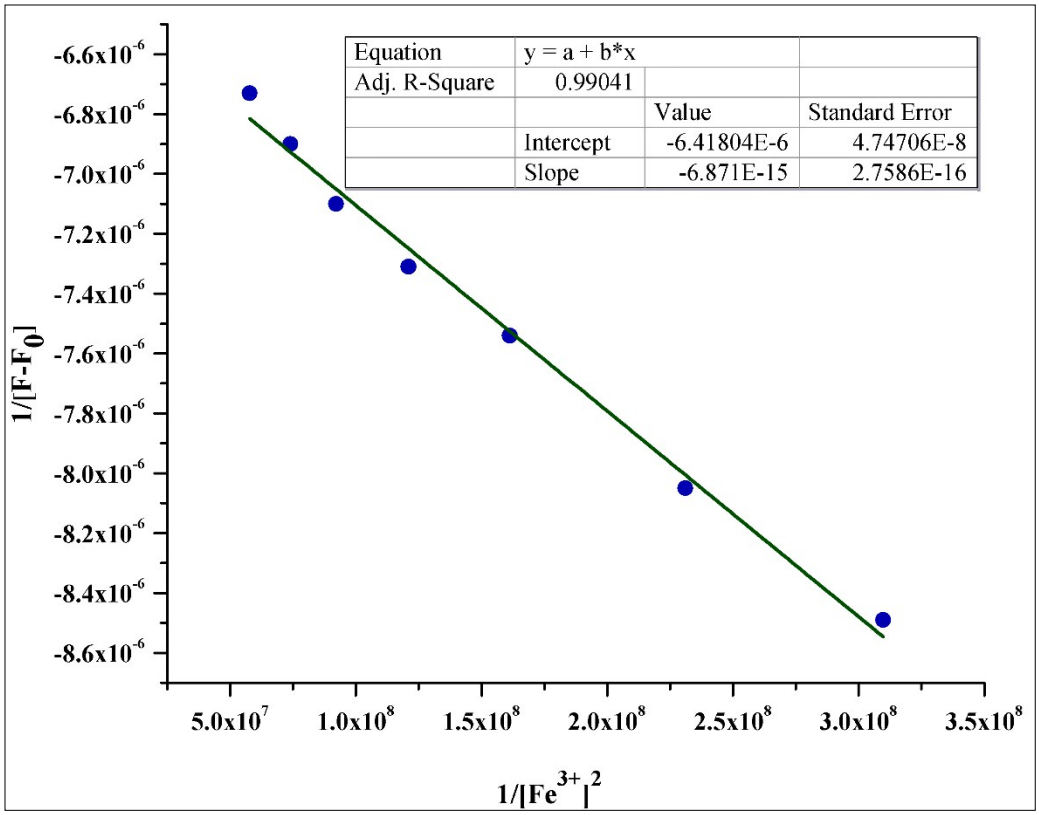

Fig. S14 Benesi–Hildebrand expression fitting of fluorescence titration curve considering 2:1 (M: L) complexation for RAPHN-Fe^{3+} at λ_{em}: 369 nm (R^2 = 0.99041).

Reagents

All reagents and chemicals were purchased from commercial suppliers and used without further purification. Analytical grade metal chloride salts of all cations were purchased from Merck Chemicals, India, 2–hydroxynaphthaldehyde, 2,6 diamino pyridine, sodium borohydride, *tetra* butyl ammonium salt of all anions from Sigma–Aldrich Chemicals, USA and solvents from Merck Chemicals (India). Milli-Q ultra pure water was used throughout all experiments.

Instruments

C, H, N contents were determined on an Exeter Analytical Inc. CHN Analyzer (Model CE–440). ^1H and ^{13}C NMR spectra were recorded on a JEOL AL–500 FT–NMR multinuclear spectrometer. $CDCl_3$ was used as a solvent with TMS as an internal standard. Chemical shifts are expressed in parts per million (ppm). Infrared spectra were recorded on Perkin Elmer FT–IR spectrophotometer in 4000–400 cm^{-1} region using KBr discs. Absorption spectra were recorded

on Shimadzu spectrophotometer, UV–1800 model. Fluorescence spectra were recorded on Horiba Jobin–Yvon Fluoromax 4 Spectrofluorometer with 5 nm slit width.

Computational details

Theoretical calculations were performed for the APHN, RAPHN and RAPHN-Fe^{3+} complex using *Gaussian-09* suit of programs.[1] Both the organic molecules i.e. APHN and RAPHN were treated as spin restricted (RB3LYP) i.e. the Becke three–parameter exchange functional in combination with the LYP correlation functional of Lee, Yang and Parr with 6-311G** basis set for all the atoms[2], while RAPHN-Fe^{3+} complex was treated as open-shell system using spin unrestricted DFT wave function UB3LYP [3] with LANL2DZ basis set.[4] DFT optimized structures were confirmed to be minima on potential energy surface (PES) by performing harmonic vibration frequency analyses (no imaginary frequency found). No symmetry constraints were applied and only the default convergence criteria were used during the geometry optimizations. Based on the optimized geometries, TDDFT calculations were also performed at the same B3LYP and UB3LYP level to calculate the electronic transition energies of RAPHN and RAPHN-Fe^{3+} complex, respectively.

References

1 M. J. Frisch, G. W. Trucks, H. B. Schlegel, G E. Scuseria, M. A. Robb, J. R. Cheeseman, G. Scalmani, V. Barone, B. Mennucci, G. A. Petersson, H. Nakatsuji, M. Caricato, X. Li, H.P. Hratchian, A. F. Izmaylov, J. Bloino, G. Zheng, J. L. Sonnenberg, M. Hada, M. Ehara, K. Toyota, R. Fukuda, J. Hasegawa, M. Ishida, T. Nakajima, Y. Honda, O. Kitao, H. Nakai, T. Vreven, J. A. Jr. Montgomery, J. E. Peralta, F. Ogliaro, M. Bearpark, J. J. Heyd, E. Brothers, K. N. Kudin, V. N. Staroverov, R. Kobayashi, J. Normand, K. Raghavachari, A. Rendell, J. C. Burant, S. S. Iyengar, J. Tomasi, M. Cossi, N. Rega, J. M. Millam, M. Klene, J. E. Knox, J. B. Cross, V. Bakken, C. Adamo, J. Jaramillo, R. Gomperts, R. E. Stratmann, O. Yazyev, A. J. Austin, R. Cammi, C. Pomelli, J. W. Ochterski, R. L. Martin, K. Morokuma, V.

G. Zakrzewski, G. A. Voth, P. Salvador, J. J. Dannenberg, S. Dapprich, A. D. Daniels, O. Farkas, J. B. Foresman, J. V. Ortiz, J. Cioslowski and D. J. Fox, Gaussian, Inc., Wallingford, CT, 2009.

2 Y. Gao, J. Shu, C. Zhang, X. Zhang, H. Chen and K. Yao, 2015, *RSC Adv*. **5**, 74629-74637.

3 P. M. Panchmatia, M. E. Ali, B. SanyaL and P. M. Oppeneer, *J. Phys. Chem. A,* 2010, **114***,* 13381–13387.

4 A. Abkari, I. Chaabane and K. Guidara, *PHYSICA E*, 2016, **81**, 136-144.